Supporting Information

Gazzola et al. 10.1073/pnas.1419335112

Normalized Bending Stiffness and Active Torque

The swimmer's dimensionless bending stiffness $b(s)$, as a function of its arc-length s, reads

$$b(s) = b_{\text{base}} + \left(b_{\text{mag}} \sqrt{s(1-s)^3} \right)^4, \qquad \text{[S1]}$$

where the parameters $b_{\text{base}} = 0.002$ and $b_{\text{mag}} = 4$ are chosen to fit the normalized experimental data by McHenry et al. (1). As normalization constant for the bending stiffness we used $\overline{B} = 5.28 \cdot 10^{-4}$ Nm^2, which is the mean value of the measurements reported in ref. 1.

The dimensionless function $F(s)$ appearing in the definition of the active torque m_a is defined as

$$F(s) = f_{\text{scale}} \left(f_{\text{base}} + \left(f_{\text{mag}} \sqrt{s(1-s)^3} \right) \right)^4 \Big), \qquad \text{[S2]}$$

where parameters are set to $f_{\text{scale}} = 0.025$, $f_{\text{base}} = 0$, and $f_{\text{mag}} = 4$. The functional form $F(s)$ is proportional to the bending stiffness $b(s)$, up to the constant b_{base}, to meet the constraint $m_a(x = 0, L) = 0$. Furthermore, such expression also satisfies the constraint $\partial_x m_a(x = 0, L) = 0$. The scaling factor f_{scale} has been set arbitrarily small to meet the small deformations assumption.

Normalized experimental data (1), bending stiffness $b(s)$, and dimensionless function $F(s)$ are reported in Fig. S1.

Derivation of Scaling Laws

Our model is naturally consistent with the universal scaling laws of macroscopic swimming (2) $Re \sim Sw^{4/3}$ for laminar swimming and $Re \sim Sw$ for turbulent swimming (with $Sw = fA_\lambda L/\nu$ being the dimensionless swimming number).

In the laminar regime, balancing the propulsive term in Eq. **15** of the main text with the viscous boundary layer drag yields

$$\rho I_3 \sim \frac{\rho u^{3/2}}{\sqrt{Re^b}}. \qquad \text{[S3]}$$

Expressing the vertical displacement as $h \sim e^{i\omega\tau}\Gamma(s)\lambda$, where $\Gamma(s)$ is an arbitrary, finite function of s, we obtain

$$I_3 = \int_0^1 n(s)\partial_s h \partial_{\tau\tau} h ds \sim \lambda^2 \omega^2. \qquad \text{[S4]}$$

Recalling that $u = U/U_b$, $Re^b = (16\epsilon^2)^{-1}(LU_b/\nu)$, $\omega = 2\pi f L/U_b$ and $\lambda = A_\lambda/L$, we can rewrite Eq. **S3** in its dimensional form as

$$\rho \frac{A_\lambda^2}{L^2} \frac{f^2 L^2}{U_b^2} \sim \rho \frac{\dfrac{U^{3/2}}{U_b^{3/2}}}{\dfrac{L^{1/2} U_b^{1/2}}{\nu^{1/2}}}, \qquad \text{[S5]}$$

which after rearranging yields

$$\frac{UL}{\nu} \sim \left(\frac{f A_\lambda L}{\nu} \right)^{4/3}, \qquad \text{[S6]}$$

that is,

$$Re \sim Sw^{4/3}, \qquad \text{[S7]}$$

consistent with ref. 2.

In the turbulent regime, balancing the propulsive term in Eq. **15** of the main text with the pressure drag yields

$$\rho I_3 \sim \rho u^2 I_1. \qquad \text{[S8]}$$

As before, expressing the vertical displacement as $h \sim e^{i\omega\tau}\Gamma(s)\lambda$, where $\Gamma(s)$ is an arbitrary, finite function of s, we obtain

$$I_1 = \int_0^1 (\partial_s h)^2 k(s) ds \sim \lambda^2. \qquad \text{[S9]}$$

Rewriting the balance Eq. **S8** in dimensional notation leads to the relation $U/L \sim f$ first discovered empirically by Bainbridge and provides a mechanistic explanation for it. By recalling that in this swimming regime A_λ/L is approximately constant (1, 3) (Fig. 2 *B* and *C* in the main text), Eq. **S8** can be rewritten as

$$Re \sim Sw, \qquad \text{[S10]}$$

also consistent with ref. 2.

Active Swimming Without Proprioception

We report a quantitative comparison between simulations of swimmers of different size (achieved by varying the bending Reynolds number) and live fish measurements by Bainbridge (3) in terms of the scaled active torque amplitude a. Simulations are carried out assuming $\rho_f = \rho_s = 1{,}000$ kg/m^3, $\nu = 10^{-6}$ m^2/s, $\rho = 300$, and $a = 1$. The bending Reynolds number is varied between $3 \cdot 10^4 \le Re^b \le 4 \cdot 10^4$ to account for different swimmer sizes. The swimming velocities and frequencies reported in Fig. 2*E* in the main text correspond to the resonant peaks exhibited by the model for an actuation wavenumber $q = 2\pi$.

The comparison of experimental data with simulations is summarized in Fig. S4, and in Fig. S5 the corresponding Strouhal numbers are reported, showing agreement with the experimental observations by Taylor et al. (4) and Bainbridge (3). Linear fits for simulations and experiments are reported in Table S1. By increasing the activation amplitude, the slope α_a of the linear fit relative to simulations approaches the experimental values observed for dace, trout, and goldfish when $a \simeq 4.75$.

Instability Owing to Delayed Feedback

To show the presence of an oscillatory instability owing to the delayed forcing we simplify the problem to eliminate the hydrodynamics by setting $\rho = 0$, $b = 1$ in Eq. **16**. This then yields

$$\partial_\tau^2 h(\tau, s) = -\partial_s^4 h(\tau, s) - \chi \partial_s^4 h(\tau - \delta, s) - \beta \partial_\tau h(\tau, s), \qquad \text{[S11]}$$

where we have added a linear damping $\beta\partial_\tau h$ to mimic the effects of hydrodynamics in a minimal setting. Without the forcing term (the second term of the right-hand side) the beam relaxes to its nonderformed configuration. The threshold for instability can be captured by investigating solution of the form $h(\tau, s) = \tilde{h} e^{iqs} e^{i\omega\tau}$. For small δ, we determine that the beam will oscillate with a frequency given by $\omega^2 \sim q^4 - 1/\delta$, as $\chi < -\beta/(q^4\delta)$. This approach

permits us to emphasize that a sufficiently large delay forcing produces lateral undulations of the fish, and furthermore selects a temporal frequency related to the resonant modes of the passive filament.

Purely Proprioceptively Driven Locomotion

In the case of proprioceptive swimmers, we solve Eqs. **15–17** of the main text after setting the active torque $m_a = 0$ and using the following invariant form for the proprioceptive feedback torque:

$$m_f(s,\tau) = \chi \partial_s^2 h(s, \tau - \delta), \qquad \textbf{[S12]}$$

where χ is the strength of the response to the stimulus $\partial_s^2 h$ and δ is a temporal delay. By following the same approach as for the active swimmer, we separate temporal and spatial variables by studying solutions of the form $h(s,\tau) = e^{i\omega\tau}\eta(s) + c.c.$, where $\omega = \Omega L/U_b$ is the leading dimensionless active angular frequency, $\eta(s) = \theta(s) + i\phi(s)$ is a complex variable, and the complex conjugate $c.c.$ ensures that h is real at all times. We, therefore, obtain a nonlinear eigenvalue problem for the velocity u and the gait $h(s,\tau)$ of the proprioceptively driven fish that reads

$$\begin{aligned}\frac{1}{\sqrt{Re^b}}\rho u^{3/2} = &-2k(s)C[\gamma]\rho u^2 \int_0^1 \left[(\partial_s\theta)^2 + (\partial_s\phi)^2\right] ds \\ &- 2k(s)C[\gamma]\rho\omega u \int_0^1 (\partial_s\phi\theta - \partial_s\theta\phi) ds \\ &+ 2n(s)\rho\omega^2 \int_0^1 (\theta\partial_s\theta + \phi\partial_s\phi) ds\end{aligned} \qquad \textbf{[S13]}$$

$$\begin{aligned}-\omega^2(1 + n(s)\rho)\eta = &-\left(b(s) + \frac{\chi b(s)}{e^{i\omega\delta}}\right)\partial_s^4\eta - k(s)u^2C[\gamma]\rho\partial_s\eta \\ &- 2\partial_s b(s)\partial_s^3\eta - \partial_s^2 b(s)\partial_s^2\eta - ik(s)uC[\gamma]\omega\rho\eta \\ &+ \frac{\partial_s^2\eta s u^{3/2}\rho}{\sqrt{Re^b}} + \frac{\partial_s\eta u^{3/2}\rho}{\sqrt{Re^b}} - \frac{\partial_s^2\eta u^{3/2}\sqrt{s}\rho}{\sqrt{Re^b}} \\ &- \frac{\chi\partial_s^2 b(s)\partial_s^2\eta}{e^{i\omega\delta}} - \frac{2\chi\partial_s b(s)\partial_s^3\eta}{e^{i\omega\delta}}.\end{aligned} \qquad \textbf{[S14]}$$

Eq. **S14** is system of eight ODEs subject to boundary conditions $\partial_s^2\eta(0,1) = 0$ and $\partial_s^3\eta(0,1) = 0$ and to the integral constraint of Eq. **S13**.

To solve this nonlinear boundary value problem, we first let $m_a = (a/2)\sin(\omega\tau)\boldsymbol{\delta}_k[x]$, effectively injecting an oscillating torque at the leading edge to induce an initial instability. Subsequently, we gradually reduce the forcing amplitude a until it vanishes, while increasing χ from zero to its designated value, implemented as a two parameter continuation scheme. As can be seen in Fig. 2 in the main text and in Fig. S2, self-propelled feedback-driven solutions exist only in the proximity of the fish's natural resonance frequencies, whereas the swimming performance is itself modulated by $\omega\delta$ and χ.

Active Swimming with Proprioception

Because in the most general case biolocomotion is produced by the simultaneous combination of central pattern generator and proprioception, we investigate this scenario by solving Eqs. **15–17** where both $m_a \neq 0$ (Eq. **8** in the main text) and $m_f \neq 0$ (Eq. **9** in the main text). By following the same approach previously outlined, we obtain a nonlinear eigenvalue problem that reads

$$\begin{aligned}\frac{1}{\sqrt{Re^b}}\rho u^{3/2} = &-2k(s)C[\gamma]\rho u^2 \int_0^1 \left[(\partial_s\theta)^2 + (\partial_s\phi)^2\right] ds \\ &- 2k(s)C[\gamma]\rho\omega u \int_0^1 (\partial_s\phi\theta - \partial_s\theta\phi) ds \\ &+ 2n(s)\rho\omega^2 \int_0^1 (\theta\partial_s\theta + \phi\partial_s\phi) ds\end{aligned} \qquad \textbf{[S15]}$$

$$\begin{aligned}-\omega^2(1 + n(s)\rho)\eta = &-\left(b(s) + \frac{\chi b(s)}{e^{i\omega\delta}}\right)\partial_s^4\eta - k(s)u^2C[\gamma]\rho\partial_s\eta \\ &- 2\partial_s b(s)\partial_s^3\eta - \partial_s^2 b(s)\partial_s^2\eta - ik(s)uC[\gamma]\omega\rho\eta \\ &+ \frac{\partial_s^2\eta s u^{3/2}\rho}{\sqrt{Re^b}} + \frac{\partial_s\eta u^{3/2}\rho}{\sqrt{Re^b}} - \frac{\partial_s^2\eta u^{3/2}\sqrt{s}\rho}{\sqrt{Re^b}} \\ &- \frac{\chi\partial_s^2 b(s)\partial_s^2\eta}{e^{i\omega\delta}} - \frac{2\chi\partial_s b(s)\partial_s^3\eta}{e^{i\omega\delta}} \\ &+ \partial_s^2\left(\frac{a}{2i}F(s)e^{-iqs}\right).\end{aligned} \qquad \textbf{[S16]}$$

Eq. **S16** is a system of eight ODEs subject to the boundary conditions $\partial_s^2\eta(0,1) = 0$ and $\partial_s^3\eta(0,1) = 0$ and the integral constraint given by Eq. **S15**.

As shown in Fig. S3, the combined effect of central pattern generator motor activation and proprioception qualitatively preserves the resonant-like response seen previously when either $m_f = 0$ or $m_a = 0$. Nevertheless, the proprioceptive term is found to quantitatively modify the output swimming velocity u, either sharpening or broadening the resonant peaks depending on the values of the parameters δ and χ. However, the detailed interplay between centralized muscle activation and proprioception is a rich and substantially unexplored problem that lies beyond the scope of this paper.

1. McHenry M, Pell C, Jr J (1995) Mechanical control of swimming speed: Stiffness and axial wave form in undulating fish models. *J Exp Biol* 198(Pt 11):2293–2305.
2. Gazzola M, Argentina M, Mahadevan L (2014) Scaling macroscopic aquatic locomotion. *Nat Phys* 10:758–761.
3. Bainbridge R (1958) The speed of swimming of fish as related to size and to the frequency and amplitude of the tail beat. *J Exp Biol* 35:109–133.
4. Taylor GK, Nudds RL, Thomas AL (2003) Flying and swimming animals cruise at a Strouhal number tuned for high power efficiency. *Nature* 425(6959):707–711.

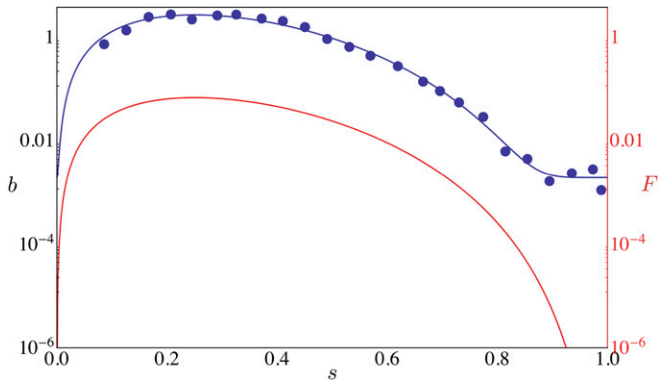

Fig. S1. Comparison between normalized experimental data (1) (blue circles), bending stiffness $b(s)$ (blue line), and dimensionless function $F(s)$ (red line).

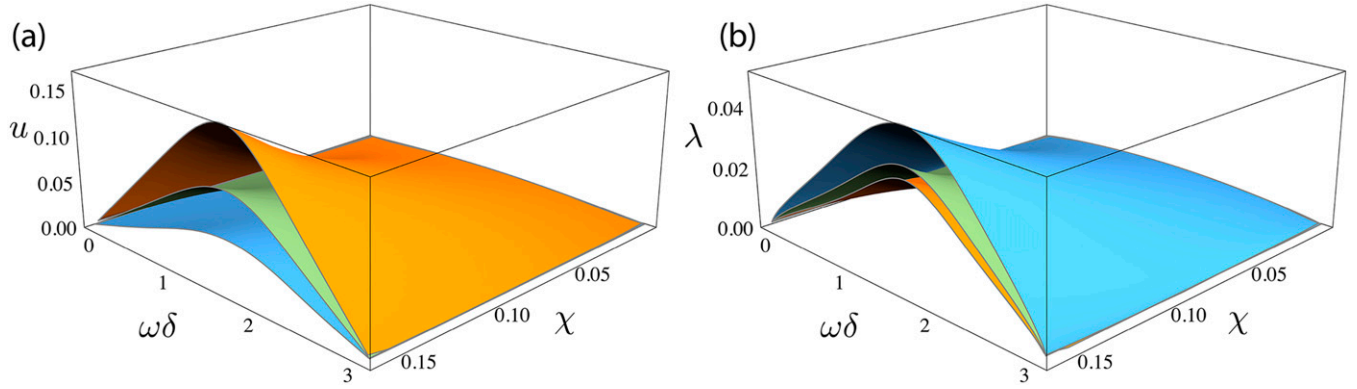

Fig. S2. Proprioceptive swimmer performance. *A* and *B* are, respectively, the locomotion velocity u and tail amplitude λ as functions of $\omega\delta$ and χ. The maximum velocity and tail amplitude are located at $\omega\delta = \pi/2$. The blue, green, and orange surfaces are associated, respectively, to the first, second, and third resonance peak. All simulations are carried out by solving Eqs. **15**–**17** of the main text with $m_a = 0$, $m_f \neq 0$ (Eq. **9** in the main text), $\rho_f = \rho_s = 1{,}000$ kg/m^3, $\nu = 10^{-6}$ m^2/s, $Re^b = 3.5 \cdot 10^4$, $\rho = 300$.

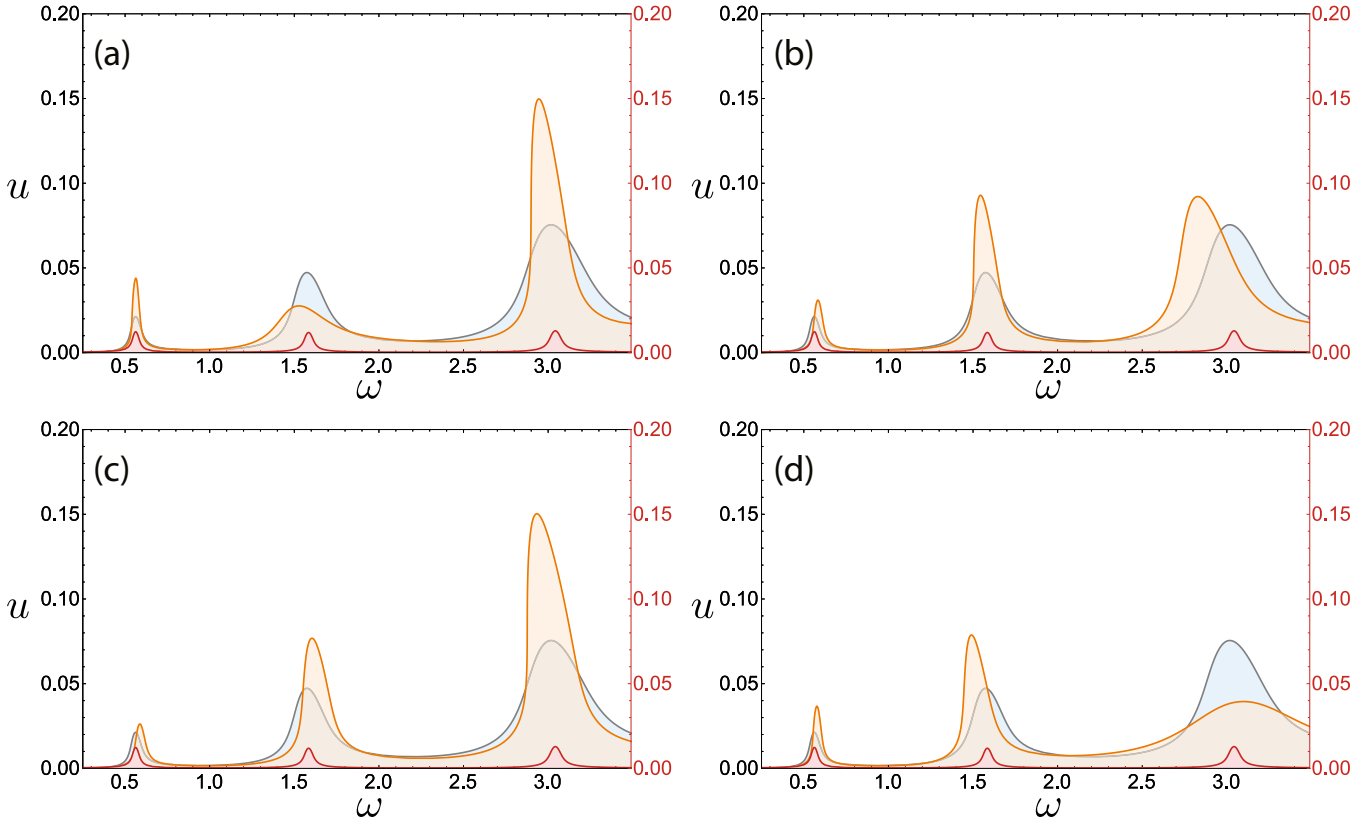

Fig. S3. Comparison between active swimmer with proprioception (orange line), active swimmer without proprioception (gray line), and the corresponding passive sheet (red line). Simulations are carried out by solving Eqs. **15**–**17** in the main text with $m_a \neq 0$ (Eq. **8** in the main text), $m_f \neq 0$ (Eq. **9** in the main text), $\rho_f = \rho_s = 1{,}000$ kg/m^3, $\nu = 10^{-6}$ m^2/s, $Re^b = 3.5 \cdot 10^4$, $\rho = 300$, $a = 1$, $q = 2\pi$, $\chi = 0.1$ and varying the delay δ. (*A*) Active swimmer with proprioception and $\delta = \pi/(2\omega_1)$, where $\omega_1 = 0.59$ is the first resonant frequency. (*B*) Active swimmer with proprioception and $\delta = \pi/(2\omega_2)$, where $\omega_2 = 1.55$ is the second resonant frequency. (*C*) Active swimmer with proprioception and $\delta = \pi/(2\omega_3)$, where $\omega_3 = 2.86$ is the third resonant frequency. (*D*) Active swimmer with proprioception and $\delta = \pi/(2\omega_4)$, where $\omega_4 = 1$ is an arbitrary non resonant frequency.

rho=300, a=4.75		w	u	lambda	f [Hz]	U [m/s]	A [m]	L [m]	U/L [Hz]	Re	St
Reb=3.5e^4	peak1	0.59	0.073	0.066	3.35	0.11	0.0028	0.042	2.62	4620	0.0844
	peak2	1.55	0.175	0.069	8.81	0.26	0.0029	0.042	6.19	10920	0.0982
	peak3	2.86	0.321	0.081	16.25	0.48	0.0034	0.042	11.43	20160	0.1152
	peak4	4.50	0.480	0.090	25.60	0.72	0.0038	0.042	17.14	30240	0.1344
Reb=3.0e^4	peak1	0.58	0.068	0.065	1.53	0.06	0.0037	0.057	1.12	3648	0.0886
	peak2	1.54	0.169	0.068	4.05	0.16	0.0039	0.057	2.77	9006	0.0994
	peak3	2.87	0.304	0.074	7.55	0.28	0.0042	0.057	4.91	15960	0.1137
	peak4	4.52	0.443	0.077	11.90	0.42	0.0044	0.057	7.37	23940	0.1244
Reb=4.0e^4	peak1	0.59	0.073	0.063	6.54	0.16	0.0020	0.032	5.06	5184	0.0814
	peak2	1.53	0.186	0.071	16.95	0.41	0.0023	0.032	12.81	13120	0.0939
	peak3	2.86	0.340	0.088	31.70	0.75	0.0028	0.032	23.44	24000	0.1190

Fig. S4. Data relative to simulations carried out by solving Eqs. **15**–**17** in the main text with $m_a \neq 0$ (Eq. **8** in the main text), $m_f = 0$, $\rho_f = \rho_s = 1{,}000$ kg/m^3, $\nu = 10^{-6}$ m^2/s, $\rho = 300$, $a = 4.75$, $q = 2\pi$, and varying $3 \cdot 10^4 \leq Re^b \leq 4 \cdot 10^4$.

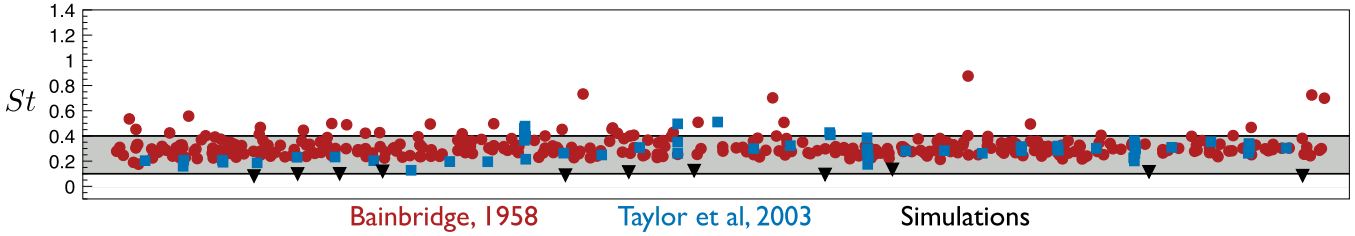

Fig. S5. Strouhal number. Red circles correspond to the experiments with trout, dace, and goldfish by Bainbridge (3). Blue squares correspond to the experimental observations by Taylor et al. (4) for both swimming and flying creatures. Black triangles correspond to simulations in the context of the present work carried out as specified in Fig. S4, by solving Eqs. **15**–**17** in the main text with $m_a \neq 0$ (Eq. **8** in the main text), $m_f = 0$, $\rho_f = \rho_s = 1{,}000$ kg/m^3, $\nu = 10^{-6}$ m^2/s, $\rho = 300$, $a = 4.75$, $q = 2\pi$, and varying $3 \cdot 10^4 \leq Re^b \leq 4 \cdot 10^4$.

Table S1. Comparison between simulations and experimental data

Linear fit: $U/L = \alpha_a \frac{\Omega}{2\pi} + \beta_a$	α_a	β_a
Dace	0.74	−1.02
Trout	0.73	−1.13
Goldfish	0.64	−0.20
Model, $a = 4.75$	0.72	−0.12

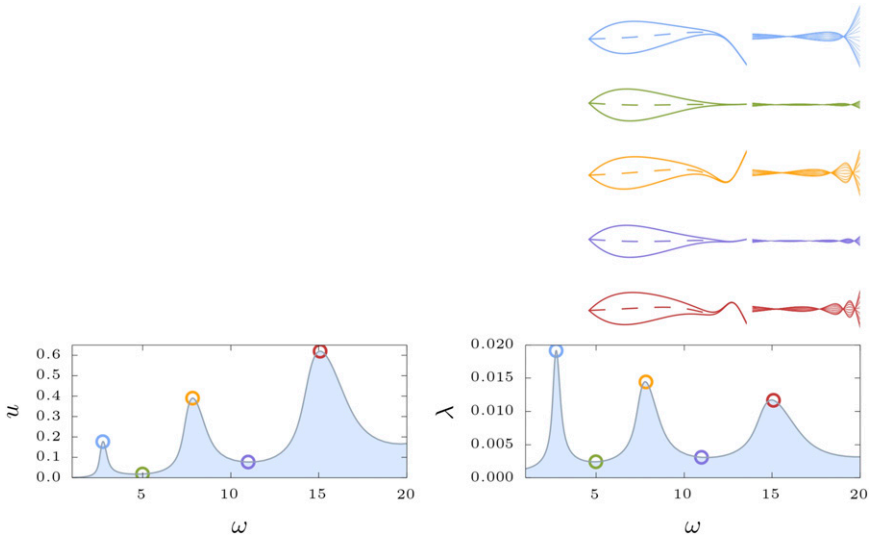

Movie S1. Active swimmers characterized by a dimensionless forcing amplitude $a = 1$ and wavenumber $q = 2\pi$, $Re^b = 10^5$, $\rho = 10$, and $m_f = 0$. The quantities u, ω, and λ represent, respectively, dimensionless velocity, forcing angular frequency, and tail amplitude. Midline motions in the vertical direction are rescaled between 0.02 L and −0.02 L.

Movie S1

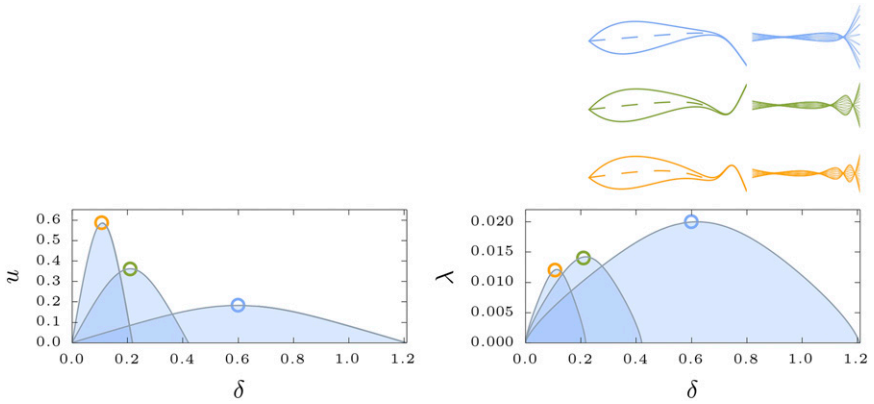

Movie S2. Proprioceptive swimmers characterized by a dimensionless feedback strength $\chi = 0.12$, $Re^b = 10^5$, $\rho = 10$, and $m_a = 0$. The quantities u, δ, and λ represent, respectively, dimensionless velocity, feedback delay, and tail amplitude. Midline motions in the vertical direction are rescaled between 0.02 L and –0.02 L.

Movie S2